SCIENCE CHINA
Life Sciences

• RESEARCH PAPERS •

June 2011 Vol.54 No.6: 535–543
doi: 10.1007/s11427-011-4172-z

Alteration of encephalomyocarditis virus pathogenicity due to a mutation at position 100 of VP1

ZHU Shu, GE XinNa, GONG XiaoWen, GUO Xin, CHEN YanHong & YANG HanChun*

Key Laboratory of Zoonosis of Ministry of Agriculture, College of Veterinary Medicine and State Key Laboratory of Agrobiotechnology, China Agricultural University, Beijing 100193, China

Received September 23, 2010; accepted March 14, 2011

Encephalomyocarditis virus (EMCV) infection leads to many diseases including encephalitis, myocarditis and diabetes in its natural host, the mouse. In this study, we generated four cDNA clones with a point mutation at position 100 of VP1. The amino acids isoleucine, alanine, serine and proline were substituted with threonine in the four different clones of EMCV strain BJC3 by site-specific mutagenesis, and viable viruses were rescued. Although all mutants and wild-type viruses display different plaque morphologies, they replicate comparably in BHK-21 cells. The pathogenicity of the mutated viruses was systematically analyzed to investigate the importance of this amino acid in the viral pathogenicity and disease phenotype of EMCV infection in mice. The results showed that the isoleucine- (T1100I) and proline-mutated viruses (T1100P) exhibited a reduced mortality, lower cerebral virus loads and alleviated brain damage while the viruses with serine (T1100S) and alanine (T1100A) substitutions displayed similar properties as the wild-type virus. These findings indicate that the amino acid at position 100 of VP1 is important for EMCV *in vivo* infection, and its mutation alters the pathogenicity of viral infection in mice.

encephalomyocarditis virus (EMCV), VP1, mutation, pathogenicity

Citation: Zhu S, Ge X N, Gong X W, *et al*. Alteration of encephalomyocarditis virus pathogenicity due to a mutation at position 100 of VP1. Sci China Life Sci, 2011, 54: 535−543, doi: 10.1007/s11427-011-4172-z

Encephalomyocarditis virus (EMCV) is a prototype member of the genus *Cardiovirus*, family Picornaviradae. EMCV can infect many vertebrates including rodents, pigs, and primates including humans [1]. Since the initial isolation of EMCV from a chimpanzee that died of acute myocarditis in 1945, a number of virus strains have been reported worldwide, especially after an outbreak of EMCV infection in swine farms in the US and European countries [2]. EMCV variants with indistinguishable serological reactions can cause clinical symptoms that are different among or even within animal species, and their pathogenicities were found to be strain-dependent [3]. Some strains of EMCV were fatal in piglets, causing acute myocarditis. In sows, EMCV caused reproductive failure leading to abortion and fetal death [4]. In mice, EMCV can cause various diseases including acute neurological disorders, diabetes and myocarditis, while some strains, like EMC-B and G424/90, generated no visible symptoms following infection [5]. To date, the mechanisms involving virulence and pathogenesis of EMCV remain unknown.

The three major capsid proteins, VP1, VP2 and VP3 that constitute the external virion shell of picornaviruses, are considered to play a pivotal role in viral infection and host recognition [6]. These proteins are so important that even a single amino acid variation can result in a profound effect on viral pathogenesis [7]. During the investigation of insulin-dependent diabetes mellitus (IDDM) in a mouse model induced by infection with EMCV variants, it was found that the amino acids at position 152 of VP1 determined the gain or loss of the diabetogenicity by affecting the effectiveness

*Corresponding author (email: yanghanchun1@cau.edu.cn)

of binding to the surface of pancreatic β-cells [8]. Furthermore, studies of Theiler's murine encephalomyelitis virus (TMEV), a 'close relative' of EMCV in the genus *Cardiovirus*, demonstrated that the amino acids on the loops exposed to the surface of the virion were important disease determinants [9].

The three-dimensional structure of Mengo virus and TMEV has been documented by X-ray crystallography, and the structural functions of the exterior surface depressions and prominent loops in viral attachment and receptor binding were analyzed and hypothesized [10]. Based on the high conformational homology of VP1 among Mengo virus, EMCV and TMEV, as well as previous results, it is postulated that the conformational change of the VP1 loop is a result of amino acid substitution, possibly contributing to different disease phenotypes in EMCV infection. Therefore, we selected the amino acid at position 100, a threonine in loop II of VP1 in EMCV, and constructed four mutated cDNA clones by introducing several single point mutations using site-directed mutagenesis. We systematically analyzed the pathogenicity of the rescued viruses to investigate the role of specific amino acids in the pathogenicity of the virus.

1 Materials and methods

1.1 Cells and virus

BHK-21 cells (China Institute of Veterinary Drug Control, Beijing, China) were maintained in Dulbecco's modified Eagle's medium (DMEM; GIBCO™, Invitrogen Corporation, Carlsbad, CA, USA) supplemented with 10% fetal bovine serum (FBS; GIBCO™, Invitrogen Corporation), 10 mmol L^{-1} Hepes, 100 mg mL^{-1} streptomycin (pH 7.4), 100 U mL^{-1} penicillin at 37°C/5% CO_2. EMCV strain BJC3 used in the study was isolated from an aborted swine fetus, from Beijing in 2005, and its genomic sequence was determined and deposited in GenBank (Accession No. DQ464062) [11].

1.2 Laboratory animals

Eight-week-old BALB/c mice (Beijing Laboratory Animal Research Centre) were used for animal trials in this study. All the animal trials were approved by the Beijing Laboratory Animal Administration Authority.

1.3 Plaque assay of virus titration

The viral titer was determined by plaque assay as described previously [12]. Dilutions of viral solutions were incubated on 80% confluent BHK-21 monolayers for 1 h at 37°C/5% CO_2. Cultures were then overlaid with 2% agarose in DMEM containing 10% FBS. The monolayers were stained for 2 d using crystal violet with the agarose layers removed.

1.4 Construction of mutated cDNA clones, production and identification of mutant viruses

The full-length infectious clone of wild-type BJC3 was constructed as described previously [13] (Figure 1A). Mutated cDNA clones were constructed by site-specific mutagenesis using a QuikChange® multi-site-directed mutagenesis kit (Stratagene) according to the manufacturer's instructions. The specific single site mutation was performed at nucleotide 2904 using mutagenic primers (Table 1). For mutagenesis, a 1.3 kb *Spe* I-*Sac* I fragment containing the mutation was digested with the respective restriction enzymes from pWSKBJC3/w and subcloned into pBluescript® II SK^+. Subsequent to site-specific mutagenesis, the mutant *Spe* I-*Sac* I fragments were digested, gel-purified and cloned back into pWSKBJC3/w to replace the corresponding fragment on the parental backbone and construct the mutated cDNA clones. These were pWSKBJC3m/I, pWSKBJC3m/A, pWSKBJC3m/S and pWSKBJC3m/P, containing the altered amino acids isoleucine, alanine, serine and proline, respectively (Figure 1B). After *in vitro* transcription, the mRNA obtained from the mutated cDNA clones were transfected into BHK-21 monolayers to generate mutant progeny viruses. This was performed as previously described [13]. The rescued viruses were identified by a common indirect immunofluorescence assay (IFA), as described elsewhere [14].

1.5 Sequencing of the single mutations in the derived viruses

BHK-21 cells infected with the mutant viruses were treated with TRIzol Reagent (GIBCO) and the extracted total RNA was reverse transcribed with Superscript™ III (Invitrogen) using the specific primers listed in Table 1. The cDNA fragments covering nt 2329–3667 (containing the mutated nucleotides) were amplified by reverse transcription-polymerase chain reaction (RT-PCR). The gel-purified PCR products were sequenced (Invitrogen, Beijing, China) to confirm the presence of the mutations.

1.6 One-step growth kinetics for the viruses

BHK-21 cell monolayers were infected at a multiplicity of infection (MOI) of 10 in 96-well plates. Following adsorption for 1 h at 37°C, the monolayers were washed three times with phosphate-buffered saline (PBS, pH 7.4), and 100 μL of complete DMEM supplemented with 2% FBS. At each time point, triplicate or quadruplicate wells were harvested and freeze-thawed three times, with total virus yields determined by plaque assay. The growth kinetics for each virus was determined twice.

1.7 Pathogenicity analyses of the EMCV variants

Sixty mice were randomly allocated to six groups (10 mice

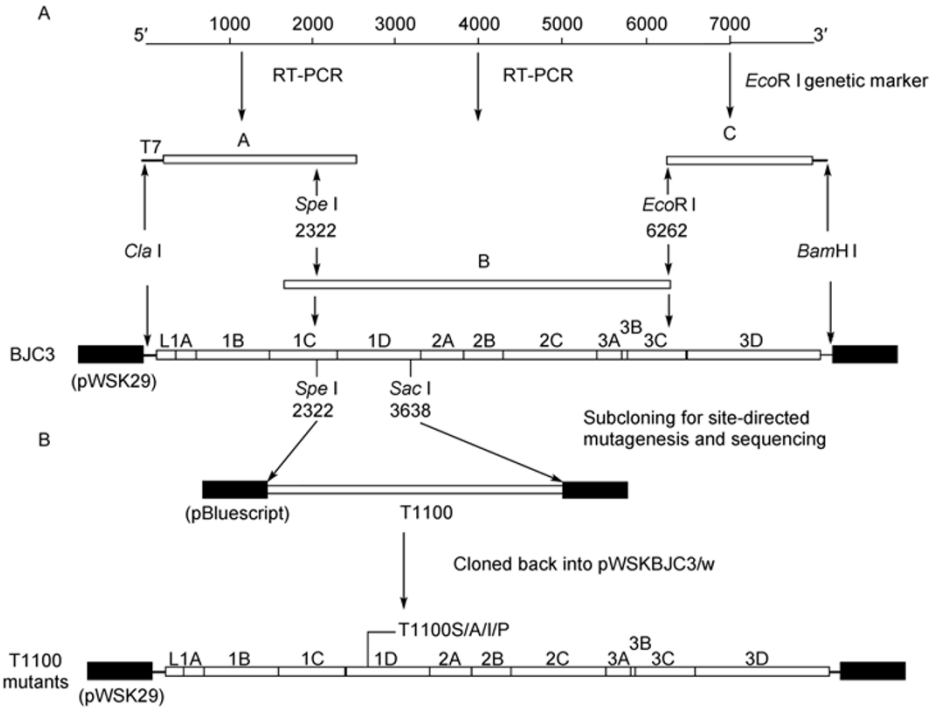

Figure 1 Schematic diagram for constructing full-length cDNA clones of BJC3 and mutant viruses. A, Capital letters (A, B and C) indicate the overlapping segments amplified from the BJC3 genome. A *Cla* I restriction site was added to the 5′ end of segments A and B to facilitate the A-B assembly and an *Eco*R I cleavage site was created by PCR mutagenesis for B-C ligation and genetic detection of rescued virus. Numbers below the restriction sites represent the nucleotide position of the BJC3 genome. B, A *Spe* I-*Sac* I segment containing the area of interest was excised from pWSKBJC3/w, cloned into pBluescript® II SK+, mutated by corresponding synthetic oligonucleotides and cloned back to construct the full length cDNA clones of mutant viruses.

Table 1 Primers used in this study

Primer[a)]	Position[b)]	Sequence (5′–3′)	Use
DetF	2637–2655	AGACGCAACTGCTGACTT	Sequencing
DetR	3498–3517	ACAATCTAACCTCCAAACC	
			Codon change
SerF		AATGGAAATGAGGAGTCCTCAAAAGTCTTTCCGC	ACC→TCC
SerR		GCGGAAAGACTTTTGAGGACTCCTCATTTCCATT	
AlaF		AATGGAAATGAGGAGGCCTCAAAAGTCTTTCCGC	ACC→GCC
AlaR		GCGGAAAGACTTTTGAGGCCTCCTCATTTCCATT	
IleF		AATGGAAATGAGGAGATCTCAAAAGTCTTTCCGC	ACC→ATC
IleR		GCGGAAAGACTTTTGAGATCTCCTCATTTCCATT	
ProF		AATGGAAATGAGGAGCCCTCAAAAGTCTTTCCGC	ACC→CCC
ProR		GCGGAAAGACTTTTGAGGGCTCCTCATTTCCATT	

a) F refers to the forward PCR primer and R stands for the reverse PCR primer. b) Numbers represent the nucleotide positions within the genome of BJC3 (GenBank accession No. DQ464062).

per group), and each group was housed separately in different isolators. Each mouse was intraperitoneally inoculated with 0.2 mL of virus containing 5×10^5 plaque forming units (PFU; high dose). The mice in the control group were administered the same volume of DMEM-2% FBS. The inoculation trial using the virus containing 2500 PFU (low dose) was designed as described above. Clinical signs in the inoculated mice were observed for two weeks post-inoculation (pi).

1.8 Virus titration in tissues of inoculated mice, histopathology and immunohistochemistry examination

Twenty-four mice were used for the inoculation trial of each rescued virus. Each mouse was infected with 0.2 mL of virus containing 2000 PFU, and six mice in each group were euthanized on days 1, 3, 5 and 7 pi. Three mice were inoculated with 0.2 mL of DMEM-2% FBS as a negative control, and were sacrificed at the end of the trial. The brains and

hearts were aseptically collected, weighed, and homogenized in DMEM-2% FBS. The homogenates were freeze-thawed three times, titrated on BHK-21 monolayers by plaque assay and genomic copy numbers of rescued viruses were quantified by quantitative real-time RT-PCR (qPCR) as described previously [14]. Total RNA was extracted from the freeze-thawed homogenates and reverse-transcribed into cDNA using Oligo-d(T). The qPCRs were performed in a reaction volume containing cDNA template, specific primers (EMCV: 5′-TGAGTCATTAGCCATTTCAACCCA-3′ and 5′-CGTGAGATACAAACCCGCCCTA-3′; β-actin: 5′-TCATCACTATTGGCAACGAGC-3′ and 5′-GAGGTCTTTACGGATGTCAACG-3′) and SYBR® Green Real-time PCR Master Mix (TOYOBA Co., Ltd., Osaka, Japan) according to the manufacturer's recommendations. The relative genomic copies of the viruses were normalized to mRNA from the β-actin gene.

Additionally, brains and hearts of the infected mice in the viral titration experiments were collected on days 3 and 5 pi, fixed in 4% buffered paraformaldehyde and embedded in paraffin. Sections were stained with hematoxylin and eosin and observed using microscopy. The extent of cellular degradation and tissue lesions was evaluated. Histological scoring of brain samples was performed as follows: 0, no visible changes; 0–1, minor changes in cell population; 1–2, meningitis, mild cellular infiltrates; 2–3, meningitis, perivascular cuffing, moderate lymphocytic infiltrates, gliosis; 3–4, local neuronal degeneration and necrosis, cerebral microvascular exudation and hemorrhage; 4–5, extensive neuronal death, diffuse encephalitis, structural disorder, tissue degradation and atrophy. The inflammatory score of the heart was determined as described elsewhere [15] (0, no lesions; 1, lesions involving <25%; 2, lesions involving 25%–50%; 3, lesions involving 50%–75%; 4, lesions involving 75%–100%).

For immunohistochemistry, cells positive for the presence of virus were detected by a standard two-step technique using a horseradish peroxidase-labeled (HRP) secondary antibody. A monoclonal antibody against VP1 was used as the primary antibody at a dilution of 1/600. Deparaffinized brain and heart sections were incubated with 10% normal goat serum for 30 min to block nonspecific binding. Diluted primary antibodies were added to the slides for 24 h at 4°C, followed by a 1/100 dilution of HRP-goat anti-mouse secondary antibody (Santa Cruz Biotechnology, Santa Cruz, CA, USA) for 30 min at room temperature. The slides were incubated with 3,3′-diaminobenzidine (DAB) substrate as prescribed and the reaction was stopped by washing the slides in PBS. After dehydration, cover slips were applied to the slides and enumeration performed by light microscopy. The number of antigen-positive cells from 10 fields of view was combined when a single section was observed and averaged over three coronal brain sections per mouse from six infected mice.

1.9 Statistical analysis

Data were expressed as mean±SD. The significance of the variability among the trials was determined by one-way or two-way analysis of variance using GraphPad Prism (version 4.0). Differences were considered statistically significant at a *P*-value less than 0.05.

2 Results

2.1 Identification of the viruses rescued from the constructed infectious cDNA clones

Viable viruses were successfully rescued from the constructed full-length wild-type cDNA clone (pWSKBJC3/w) of BJC3 and its mutated cDNA clones (pWSKBJC3m/I, pWSKBJC3m/A, pWSKBJC3m/S and pWSKBJC3m/P) after *in vitro* transfection on BHK-21 cells. The rescued virus from the wild-type cDNA clone was designated as RvBJC3W, and the viruses rescued from the four mutated cDNA clones were individually designated as T1100I, T1100A, T1100S and T1100P. All the rescued viruses could replicate stably and generate typical cytopathic effects (CPEs) in BHK-21 cells. BHK-21 cells infected with the rescued viruses were stained with a monoclonal antibody specific for the VP1 of EMCV (Figure 2A). To evaluate the genetic stability of each point mutation following passage, we performed four consecutive passages of the rescued viruses in BHK-21 cells. The presence of the mutated nucleotides for each rescued virus was confirmed by sequencing the amplified fragment from RT-PCR (data not shown).

2.2 Rescued wild-type and mutant viruses replicate similarly in BHK-21 cells with different plaque morphology

To determine whether the EMCV replication *in vitro* could be affected by amino acid substitutions, we performed virus plaque assays and one-step growth kinetics in BHK-21 cells. Compared with RvBJC3W, the four mutant viruses showed differences in plaque size. Serine- (T1100S) and alanine-mutated (T1100A) viruses produced larger plaques with a size of 8–10 mm, similar to RvBJC3W. Isoleucine- (T1100I) and proline-mutated (T1100P) viruses generated approximately 60% smaller plaques, with a size of 4–5 mm (Figure 2B). One-step growth kinetic assays indicated that the four mutant viruses exhibited growth curves similar to RvBJC3W (Figure 2C).

2.3 Rescued mutant viruses T1100I and T1100P caused a reduced mortality in mice

To analyze the virulence of mutant variants, eight-week-old male BALB/c mice were intraperitoneally inoculated with the mutated viruses, and the survival rates were observed.

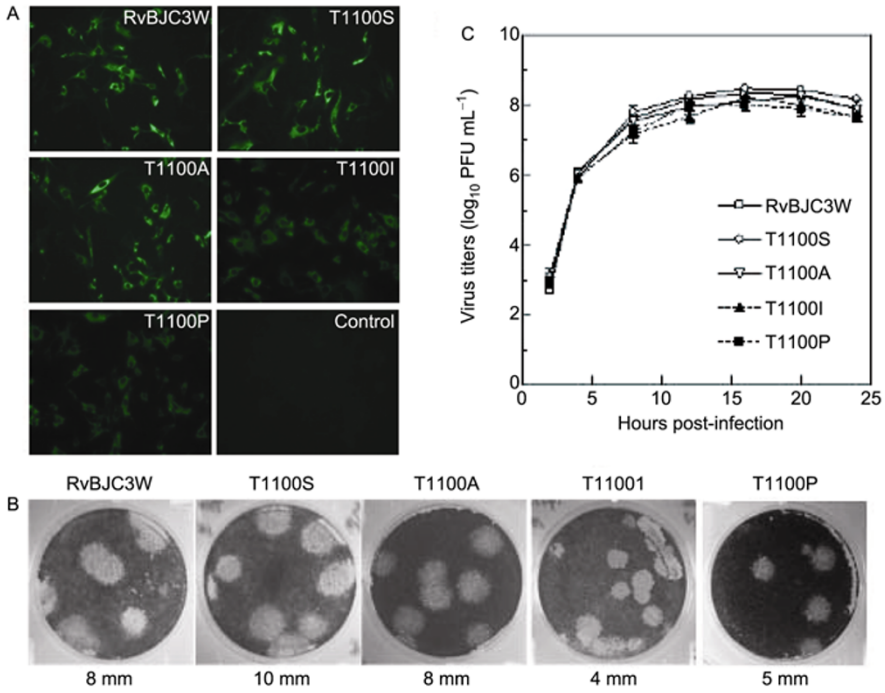

Figure 2 Replication of RvBJC3W and mutant viruses in BHK-21 cells. A, IFA identification of the parental and mutant viruses. BHK-21 cells were infected with viruses at an MOI of one and incubated with a VP1 monoclonal antibody at 6 h post-infection. B, Plaque morphology of the rescued viruses. C, One-step growth curve of the rescued viruses. The viral titers were determined by plaque assay. The growth curves of different viruses were comparable (P>0.05). The data shown are mean±SD (error bars) for triplicate independent trials.

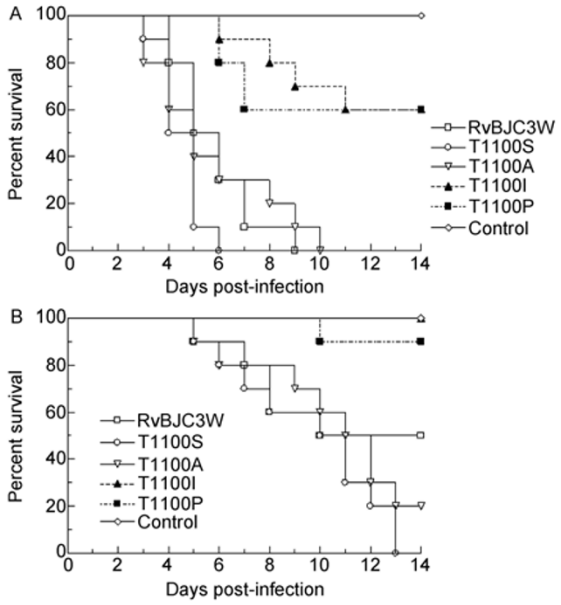

Figure 3 Survival curves of mice inoculated with the rescued viruses (n=10). A, Inoculation of 5×10^5 PFU of virus. B, Inoculation of 2500 PFU of virus.

Under the high dose conditions, mice inoculated with RvBJC3W, T1100S and T1100A developed clinical signs within two days pi and began to die on days 3 (T1100S, T1100A) and 4 (RvBJC3W) pi. All mice died within 10 days pi, while mice inoculated with T1100I and T1100P had a survival rate of 60% at the end of the two-week observation period despite similar clinical symptoms (Figure 3A). For the low dose groups, the onset of encephalitic symptoms was delayed. The first death in RvBJC3W-, T1100S- and T1100A-infected groups occurred on day 5 pi and the mortality rate in these three groups was 50%, 100% and 80%, respectively, over the two week observation period. T1100I- and T1100P-infected mice barely had visible abnormal clinical reactions, and presented a survival rate of 100% and 80%, respectively (Figure 3B). The survival rate of mice infected with T1100I was significantly higher than that of RvBJC3W-infected mice at the high (P<0.0001) and low dose (P<0.0001) challenges. T1100P-infected mice also showed significantly lower mortality rate than RvBJC3W under high (P=0.0016) and low dose (P=0.0036) conditions. In addition, no significant survival differences were observed among RvBJC3W-, T1100S- and T1100A-infected mice (P>0.5). All mice in the control group remained healthy and survived the entire experimental period. These data indicate that the isoleucine- and proline-mutations resulted in obviously reduced pathogenicity of EMCV BJC3 in mice.

2.4 Rescued mutant viruses T1100I and T1100P exhibited lower virus loads in the target organs of inoculated mice

To examine the extent of the replication of mutant viruses *in*

vivo, we infected the BALB/c mice and determined the levels of infectious viruses in their brains and hearts on days 1, 3, 5 and 7. Mice were intraperitoneally inoculated with 2000 PFU of each rescued virus. The RvBJC3W-, T1100S- and T1100A-infected mice developed neurological disorders after day 5 pi, but no mortality was observed within 7 d. No obvious clinical signs were observed in T1100I- and T1100P-infected groups. As shown in Figure 4A, the viral titers in T1100I- and T1100P-infected mice were undetectable by plaque assay on day 1 pi while viruses in T1100S- and T1100A-infected mice could be titrated. Compared with the parental RvBJC3W, T1100S-infected mice had significantly higher viral loads in brains on days 1 and 3 pi (P<0.001, P<0.05), whereas T1100I- and T1100P-infected mice had significantly lower viral loads in the brains on days 3, 5 and 7 pi (P<0.001). Viral titers in the brains of T1100I- and T1100P-infected mice were approximately 100–10000-fold lower than that of RvBJC3W-infected mice on days 3 and 7 pi. Viral genomic RNA levels in the brains of the infected mice showed similar tendencies (Figure 4C). The number of genomic copies of T1100S in the brains of infected mice was significantly higher than that of parental RvBJC3W-infected mice on days 1 and 3 pi (P<0.05). The T1100I- and T1100P-infected mice contained a lower number of genomic copies compared with parental RvBJC3W-infected mice (P<0.001). The viral titers of parental and mutant viruses decreased on day 7 pi (Figure 4A), and may be due to an increase in the titer of antibodies against viruses, as previously reported in a study on the diabetogenic EMC-D strain [16]. By contrast, the viral loads in the hearts showed no differences among the mice infected with the rescued viruses (Figure 4B and D). Viral loads and genomic copies were not detected in control mice. These data revealed that the significant differences in viral loads in the brains of infected mice had a strong correlation with the observed mortalities.

2.5 Mutated T1100I and T1100P showed alleviated cerebral tissue lesions in mice

To determine whether the isoleucine and proline mutations prevent virus dissemination and restrict virus-induced tissue damage, we performed histological examinations of the target organs in infected mice. Histopathological changes were observed in the cerebral cortex, hypothalamus and hippocampus of brains. In the mice infected with RvBJC3W, T1100S and T1100A, severe and concentrated neuronal damage including nuclei pyknosis, degeneration, necrosis

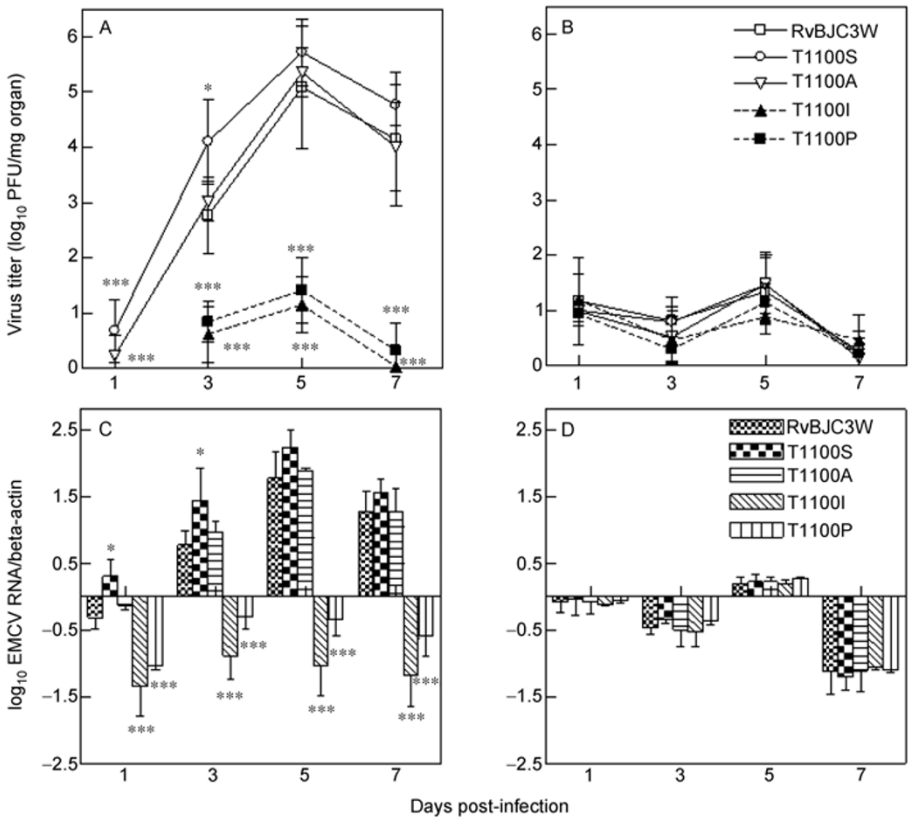

Figure 4 Titration of parental RvBJC3W and mutant viruses in target organs of mice inoculated with the rescued viruses. Viral titers in target organs were determined by plaque assay. A, Viral titers in brains of the inoculated mice. B, Viral titers in hearts of the inoculated mice. Viral genomic RNA levels were determined by quantitative real-time RT-PCR. C, Viral genomic RNA levels in brains. D, Viral genomic RNA levels in hearts. Data are expressed as mean±SD (error bars) (n=6). *, P<0.05; ***, P<0.001, compared with RvBJC3W.

and degradation (Figure 5A) was observed. By contrast, light and sporadic pathological changes, such as mild meningitis, microvascular hemorrhaging and perineural space broadening could be observed in the cerebral cortex of T1100I and T1100P-infected mice (Figure 5B). Detailed histopathological scores are shown in Figure 6A. Although T1100S-infected mice had more severe brain damage compared with parental RvBJC3W-infected mice on day 3 pi (P<0.05), no significant differences in the overall distribution and severity of the cerebral lesions were observed in T1100S- and T1100A-infected mice. By contrast, in T1100I- and T1100P-infected mice, degeneration and necrosis of neurons were barely seen on day 3 pi (P<0.01) and only moderate inflammatory reactions could be seen on day 5 pi (P<0.001), indicating that T1100I and T1100P caused less brain damage than RvBCJ3W. Histopathological examination of the heart sections revealed that all inoculated mice had very mild myocarditis, including mononuclear cell infiltration in a few and very modest myocardium lesions (data not shown). The lesion score was under one and showed no significant differences among all inoculated groups.

Viral antigen localization and enumeration were performed by immunohistochemistry. The results showed that positive cells in RvBJC3W-, T1100S- and T1100A-infected mice were concentrated and localized in the pyramidal cell

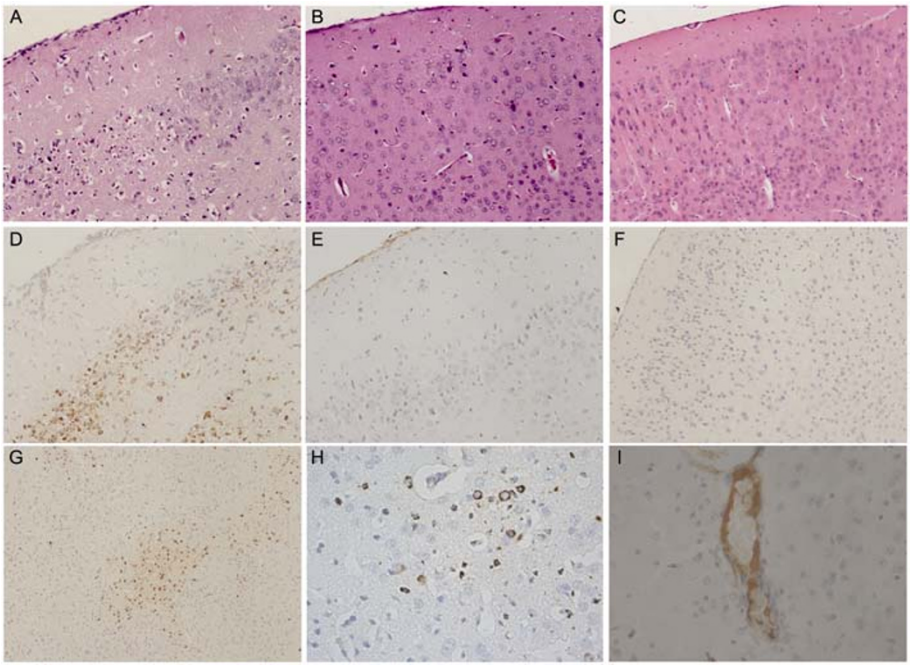

Figure 5 Neuropathology and immunohistochemistry of cerebral tissues in mice infected with the rescued virus. A and B, Pathological changes of T1100S and T1100I, respectively, on day 5 pi. D and E, Immunohistochemistry at the same infectious sites for T1100S and T1100I on day 5 pi. C and F, Control sections. G, Concentrated positive signals in local necrotic foci. H, Neurons were mostly, cytoplasmic staining of neurons. I, Antigen-positive signals in the endotheliocytes of capillaries. G–I, T1100S on day 3 pi. Magnification: A–F, ×200; G, ×100; H and I, ×400.

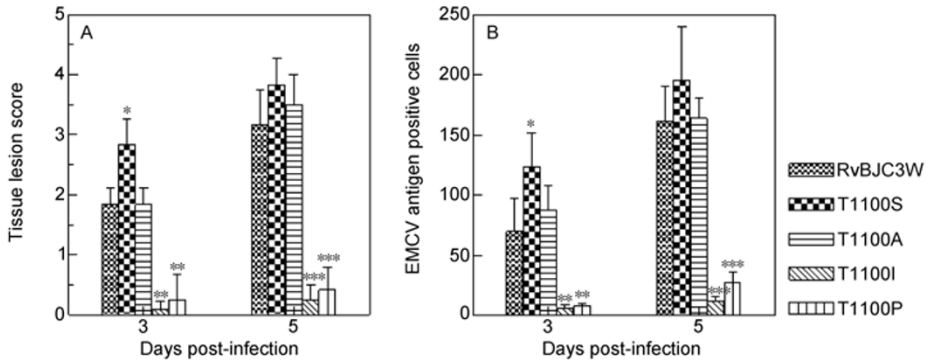

Figure 6 Cerebral histopathological scores of mice infected with the rescued viruses. A, Histopathological evaluation of cerebral lesions. B, Detection of EMCV antigen-positive cells in the brains by immunohistochemistry. Data are expressed as mean±SD (error bars) (n=6). *, P<0.05; **, P<0.01; ***, P<0.001.

layer of cerebral cortices on day 3 pi (Figure 5D and G), while positive cells in T1100I- and T1100P-infected mice were hardly observed (Figure 5E). Viral antigens were found in either microglial cells or macrophages; however, neurons in the cerebral hemisphere of RvBJC3W-, T1100S- and T1100A-infected mice were mostly affected (Figure 5H). Positive signals were also seen in the endotheliocytes of capillaries in the cerebral cortex (Figure 5I). On day 5 pi, more and stronger positive signals were found in RvBJC3W-, T1100S- and T1100A-infected mice, whereas only a few positive cells were seen in T1100I- and T1100P-infected mice. Positive cell enumeration showed significantly more infected neural cells in RvBJC3W-, T1100S- and T1100A-infected mice on day 3 ($P<0.01$) and 5 ($P<0.001$) pi (Figure 6B).

3 Discussion

3.1 Selection of animal model and position for site-directed mutagenesis

Our previous studies indicated that strain BJC3 used in this study was fatal to mice because of its strong neurovirulence, but not to piglets [17]. Thus, analyzing the associated molecular mechanisms for pathogenicity was essential using a mouse model. Because the amino acid sequence of VP1 for EMCV BJC3 shared 96.4% homology with that of Mengo virus, these two viruses have remarkable similarity with respect to conformational structure of their capsid protein. Thus, the already known VP1 structure of Mengo virus could be used as a substitution analogy for a BJC3 VP1 molecular model. In addition, the structural comparison between Mengo virus and TMEV, a well-investigated virus for CNS disease models, showed a similar conformation of loop II (residues 94–112 in TMEV and 90–110 in Mengo virus) on the external surface of the virion [18]. Based on the reported structures for Mengo, molecular modeling analysis by Collaborative Computational Project No. 4 (CCP4; version 6.11) indicates that EMCV VP1 loop II is on the periphery of a deep depression on the surface of the virion that has been proposed as a probable receptor binding site and the threonine is at the top. Previous evidence has shown that Thr-101 of TMEV VP1 is a disease determinant [19]. Therefore, we focused on the threonine at position 100 of VP1 in BJC3 as the target of mutagenesis. Among all possible mutations, by changing the first and second base of the original ACC codon, we selected serine, alanine, isoleucine and proline as representatives of different chemical traits. Similar to threonine, serine is also classified as a polar amino acid bearing a hydroxyl group. Alanine is a small nonpolar aliphatic amino acid. Another hydrophobic amino acid, isoleucine, was chosen as mutation existing naturally at the same site in VP1 of Mengo viruses and led to a conformational change that conferred an ability to avoid monoclonal antibody neutralization [20]. The proline mutation is an attempt to act as a structural disruptor for possible ring formation.

3.2 Amino acid substitutions altered the *in vivo* replication of EMCV in mice

Although the mutant viruses showed similar one-step growth curves, the different plaque size might be an implication of altered replicative efficiency and lytic ability in BHK-21 cells between mutated variants. It was further reflected in the *in vivo* viral loads that the mutant viruses, T1100S and T1100A, with larger plaque size, maintained completely efficient replication in mice brains, similar to the rescued wild-type virus RvBJC3W. The smaller plaque forming mutant viruses, T1100I and T1100P, showed significantly deficient cerebral growth. Despite the viral titers of mutant viruses displaying no significant differences in the mouse heart, we cannot exclude the possible influence of viral replication on myocardial tissues. All mutant viruses, as well as the parental wild-type RvBJC3W, replicated at an extremely low level in hearts. It seems that the BJC3 strain has poor myocardial proliferation, similar to some previously reported EMCV isolates [3]. The discrepancy between *in vivo* and *in vitro* kinetics might be related to the different virus receptor(s) on BHK-21 cells and mice target cells, as suggested previously with TMEV variants [21]. Further histological analyses demonstrated an obvious correlation between damage in target organs, overall *in vivo* replication, and certain strain-dependent properties.

3.3 Amino acid mutations possibly alter virus replication in certain cerebral cells

Immunohistochemistry results revealed that the viral replication of highly pathogenic mutants like T1100S and T1100A in the cerebral cells, especially the neurons, resembled that observed for wild-type virus. By contrast, the replication of less pathogenic mutants in neurons appears to be minimal, suggesting that the infection/replication of T1100I and T1100P might be severely compromised in neurons *in vivo*. Combined with the disparity of viral load in the brains and hearts of infected mice, a more feasible explanation for the different pathologies of T1100 mutants would be altered viral replication in mouse cerebral cells, especially neurons, attributable to the single amino acid substitution. Thus, we hypothesize that the threonine at position 100 of VP1 likely participates in viral interaction of neuronal cells and somehow influences viral proliferation and spread in the brain. The actual mechanism associated with this alteration in pathogenicity alteration requires further exploration. Viruses with isoleucine and proline mutations appear to have a reduced ability to grow in the brains of infected mice, but cause mortality when inoculated at a high dose. Unlike Ala^{152} of VP1, which is a determinant of viral infection for

pancreatic β-cells and gain or loss of diabetogenicity in EMC-D [7], it seems that Thr^{100} in BJC3 VP1 is not the only factor determining the EMCV cerebral replication and viral pathogenicity.

4 Conclusion

Our findings provide direct evidence that substitutions of the amino acid at position 100 of VP1 could influence the pathogenicity of EMCV BJC3 by affecting viral replication in the brain, especially in neurons, of infected mice.

This work was supported by the National Natural Science Foundation of China (Grant No. 30530550) and the Program for Innovative Research Team in University of China (Grant No. IRT0866).

1 LaRue R, Myers S, Brewer L, *et al*. A wild-type porcine encephalomyocarditis virus containing a short poly(C) tract is pathogenic to mice, pigs, and cynomolgus macaques. J Virol, 2003, 77: 9136–9146
2 Kassimi L B, Boutrouille A, Gonzague M, *et al*. Nucleotide sequence and construction of an infectious cDNA clone of an EMCV strain isolated from aborted swine fetus. Virus Res, 2002, 83: 71–87
3 Cerutis D R, Bruner R H, Thomas D C, *et al*. Tropism and histopathology of the D, B, K, and MM variants of encephalomyocarditis virus. J Med Virol, 1989, 29: 63–69
4 Koenen F, Vanderhallen H, Papadopoulos O, *et al*. Comparison of the pathogenic, antigenic and molecular characteristics of two encephalomyocarditis virus (EMCV) isolates from Belgium and Greece. Res Vet Sci, 1997, 62: 239–244
5 Psalla D, Psychas V, Spyrou V, *et al*. Pathogenesis of experimental encephalomyocarditis: a histopathological, immunohistochemical and virological study in mice. J Comp Pathol, 2006, 135: 142–145
6 Whitton J L, Cornell C T, Feuer R. Host and virus determinants of picornavirus pathogenesis and tropism. Nat Rev Microbiol, 2005, 3: 765–776
7 Jun H S, Kang Y, Notkins A L, *et al*. Gain or loss of diabetogenicity resulting from a single point mutation in recombinant encephalomyocarditis virus. J Virol, 1997, 71: 9782–9785
8 Jun H S, Kang Y, Yoon H S, *et al*. Determination of encephalomyocarditis viral diabetogenicity by a putative binding site of the viral capsid protein. Diabetes, 1998, 47: 576–582
9 Jnaoui K, Minet M, Michiels T. Mutations that affect the tropism of DA and GDVII strains of Theiler's virus *in vitro* influence sialic acid binding and pathogenicity. J Virol, 2002, 76: 8138–8147
10 Luo M, Vriend G, Kamer G, *et al*. The atomic structure of Mengo virus at 3.0 A resolution. Science, 1987, 235: 182–191
11 Zhang G Q, Ge X N, Guo X, *et al*. Genomic analysis of two porcine encephalomyocarditis virus strains isolated in China. Arch Virol, 2007, 152: 1209–1213
12 Hertzler S, Luo M, Lipton H L. Mutation of predicted virion pit residues alters binding of Theiler's murine encephalomyelitis virus to BHK-21 cells. J Virol, 2000, 74: 1994–2004
13 Zhang G Q, Zhu S, Ge X N, *et al*. Construction of full-length infectious clone for encephalomyocarditis virus BJC3 and identification of rescued virus (in Chinese). Acta Veterinaria et Zootechnica Sinica, 2009, 40: 1350–1357
14 Jia H, Ge X, Guo X, *et al*. Specific small interfering RNAs-mediated inhibition of replication of porcine encephalomyocarditis virus in BHK-21 cells. Antiviral Res, 2008, 79: 95–104
15 Hardarson H S, Baker J S, Yang Z, *et al*. Toll-like receptor 3 is an essential component of the innate stress response in virus-induced cardiac injury. Am J Physiol Heart Circ Physiol, 2007, 292: H251–258
16 Yoon J W, McClintock P R, Onodera T, *et al*. Virus-induced diabetes mellitus. XVIII. Inhibition by a nondiabetogenic variant of encephalomyocarditis virus. J Exp Med, 1980, 152: 878–892
17 Ma L, Ge X N, Zhang J L, *et al*. Pathogenicity analysis of Chinese isolates of encephalomyocarditis virus (in Chinese). Chin J Vet Med, 2008, 44: 20–21
18 Luo M, He C, Toth K S, *et al*. Three-dimensional structure of Theiler murine encephalomyelitis virus (BeAn strain). Proc Natl Acad Sci USA, 1992, 89: 2409–2413
19 Zurbriggen A, Thomas C, Yamada M, *et al*. Direct evidence of a role for amino acid 101 of VP-1 in central nervous system disease in Theiler's murine encephalomyelitis virus infection. J Virol, 1991, 65: 1929–1937
20 Boege U, Kobasa D, Onodera S, *et al*. Characterization of Mengo virus neutralization epitopes. Virology, 1991, 181: 1–13
21 Myoung J, Hou W, Kang B, *et al*. The immunodominant $CD8^+$ T cell epitope region of Theiler's virus in resistant C57BL/6 mice is critical for anti-viral immune responses, viral persistence, and binding to the host cells. Virology, 2007, 360: 159–171